Journal of Engineering Mathematics **40:** 333–353, 2001.

Forced vibrations of a body supported by viscohyperelastic shear mountings

A. E. ZÚÑIGA* and M. F. BEATTY
Department of Engineering Mechanics, University of Nebraska-Lincoln, Lincoln, NE 68588-0526, U.S.A.

Received 19 July 2000; accepted in revised form 6 January 2001

Abstract. The damped, finite-amplitude forced vibration of a rigid body supported symmetrically by simple shear springs and by a smooth inclined bearing surface is studied. The spring material is characterized as a compressible or incompressible, homogeneous and isotropic viscohyperelastic material for which the shear response function in a simple shear deformation is a quadratic function of the amount of shear. The trivial case of constant shear response is included. The equation for the damped motion of the load is a nonlinear, ordinary differential equation of the forced Duffing type with a constant static shift term due to gravity, and for which an exact solution is unknown. An approximate solution is obtained by the method of harmonic balance. Results for the motion of the load relate the system design parameters to the amplitude-frequency response and to the amplitude-driving force intensity response of the system. Regions of stable motion are identified in terms of the amplitude of the motion, driving-force intensity, driving frequency, and system design parameters. Geometrical characterizations of the motion are related schematically to certain cross-sections through the full three-dimensional solution surfaces for the amplitude and for the phase of the motion. A simple diagram maps the loci of all bifurcation points against the static shear deflection, which serves as the system design parameter for the inclined motion. An infinitesimal stability analysis shows that the bifurcation points of the inclined motion fall on the stability boundaries of the numerical solution of a three-parameter Hill equation. The solution provides information that illustrates how the system design parameters affect the motion of the load and how these may be chosen to control the amplitude of the oscillations and the stability of the system. The results are valid for all compressible or incompressible, homogeneous and isotropic, viscohyperelastic materials in the aforementioned class.

Key words: nonlinear elasticity, Duffing equation, harmonic balance, stability, Mathieu-Hill equations

1. Introduction

It is well-known that rubber shear mounts can sustain substantial deflections under severe time-varying loads due to impact and vibration. At the same time, the damping properties of the rubberlike material serve to mitigate such loading effects by providing natural vibration absorption through energy dissipation. Consequently, in analysis of the motion of a load supported by rubber shear mountings, it is anticipated that both finite deformation of the shear blocks and internal viscous damping properties of the elastomer share importance. While the shear response of elastomers generally is nonlinear, experiments show that simple shear springs exhibit the atypical property of linear shear response for angles of shear up to roughly 25° for soft rubbers, and somewhat smaller angles for hard rubbers [1]; also [2, Chapter 35] and [3, Section 4.3]. On the other hand, much larger packaging shock deflections and vibration amplitudes are not uncommon. In fact, deflections up to twice the thickness of the shear block, an angle of shear exceeding 60°, are reported [4, Chapter 7]; and beyond 25°, tests show that

*Current address: Departamento de Ingeniería Mecánica, Instituto Technologico y de Estudios Superiores de Monterrey, E. Garza Sada 2501 Sur, C.P. 64849, Monterrey, N.L., Mexico.

the shear stress response becomes increasingly nonlinear [1], [2, p. 35.18]. Bearing in mind that a great fraction of the deflection may be due to static loading alone, investigation of the finite amplitude vibration of a load supported by simple shear springs operating beyond, but perhaps close to the linear range of shear response is especially relevant. For, even though the nonlinear variation in material properties, in this instance the shear response function, may be small, the nonlinearity can produce undesirable dynamical effects on the motion. Our objective here is to study the nonlinear, damped, finite-amplitude forced vibration of a load supported by simple shear springs operating in the near-linear range of shear response.

An extensive study of the free and forced, but undamped vibration of a load on simple shear springs characterized by compressible and incompressible, isotropic hyperelastic material response has been carried out by Beatty and co-workers [5]–[10]. To capture the mechanical behavior in the near-linear range of the nonlinear material, a shear-response function quadratic in the amount of shear, a model based on the general, nonlinear constitutive relation for the isotropic elastic shear-response function, is introduced. This leads to an equation of motion of the Duffing type for both free and driven oscillations. In the former case, the solution is obtained exactly in terms of a Jacobian elliptic function [5], while the approximate method of harmonic balance is used in [10] to study the undamped forced vibrational motion of the system. It is shown that the approximate solution for the driven-vibration case provides useful information that illustrates how the system design parameters affect the motion of the load and how these may be chosen to control the amplitude of the oscillations and the system stability. Effects of damping on the free vibrations of the load, based on a constitutive equation for an isotropic, viscohyperelastic material have been studied by Beatty and Zhou [11, 12]. The model having quadratic shear response in [12] leads to an equation of the damped Duffing class, and the approximate solution is therein described by the method of slowly varying amplitude and phase.

In this paper, we study the effects of the nonlinear elastic material response on the damped, finite-amplitude forced vibration of a load supported symmetrically by shear springs of the flat, sandwich plate variety that initially are stress-free, undeformed, and undergo ideal simple shear deformations. The load is also supported by a smooth, inclined bearing surface parallel to the plane of shear. For the class of viscohyperelastic materials having a quadratic shear-response function, the equation of motion of the load is described by a forced Duffing equation for which an approximate solution is obtained by the method of harmonic balance. We focus on the physical content of the results and also explore stability of the harmonic solution of this equation. Results for the motion of the load relate the system design parameters to the amplitude-frequency response and to the amplitude-driving force intensity response of the system. Regions of stable motion are identified in terms of the amplitude of the motion, driving-force intensity, driving frequency, and system design parameters. Geometrical characterizations of the motion are related schematically to certain cross-sections through the full three-dimensional solution surfaces for the amplitude and for the phase of the motion described in the general analysis due to Holmes and Rand [13]. A simple bifurcation diagram maps the loci of all bifurcation points against the static shear deflection, which serves as the system design parameter for the inclined motion. An infinitesimal stability analysis shows that the bifurcation points of the inclined motion fall on the stability boundaries of the numerical solution of a three-parameter Hill equation, which for a horizontal motion reduces to the Mathieu equation.

We begin in Section 2 with a description of the problem and the formulation of the equation of motion. The problem solution by harmonic balance is described in Section 3. In Section

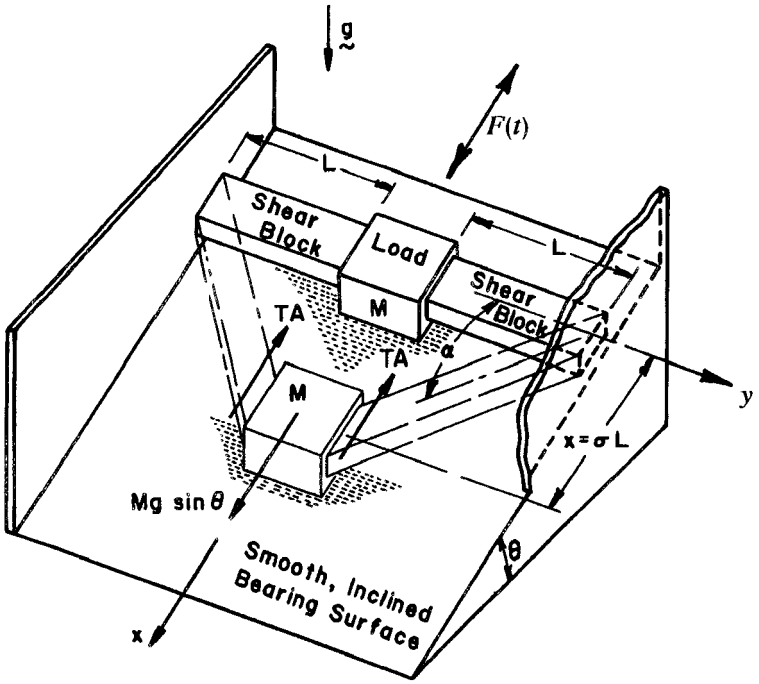

Figure 1. Schematic of the nonlinear oscillator.

4, the amplitude-frequency response and the amplitude-driving force response are described graphically to relate the system design parameters to the motion of the system and to its bifurcation at points of instability. Infinitesimal stability of the harmonic solution is examined. Bifurcation points of the inclined motion are now exhibited as points on the stability boundaries of the numerical solution of the three-parameter Hill equation. We focus throughout on the physical content of the results.

2. Formulation of the problem

Let us consider a rigid body of mass M, called the load, supported symmetrically by compressible or incompressible, homogeneous and isotropic viscohyperelastic shear blocks of original length L and cross-sectional area A. The shear blocks are bonded to the load at one face and to parallel rigid supports at the other. We suppose that the load is supported on a smooth, bearing surface inclined at an angle θ with the horizontal plane and parallel to the plane of shear, as shown in Figure 1.

The inertia of the shear springs will be neglected, as usual; and effects due to symmetrical bending of the shear mounts will be ignored. We thus consider that each shear block executes an ideal isochoric, time-dependent simple shear deformation of amount $\sigma(t) = \tan\alpha(t)$, where $\alpha(t)$ is the current angle of shear at time t measured from the initial, undeformed state shown in Figure 1. Let $T_{12}(\sigma, \dot{\sigma})$ denote the Cauchy shear stress exerted on each shear spring due to M, and recall that the cross sectional area A of each shear mount is preserved in a simple shear. The viscous effect is indicated by the stress dependence on the shearing rate $\dot{\sigma} \equiv \mathrm{d}\sigma(t)/\mathrm{d}t$. Then the total force acting on the load is due to the restoring shear force $\hat{T}(\sigma, \dot{\sigma}) \equiv -AT_{12}(\sigma, \dot{\sigma})$ exerted by each shear spring, the gravitational component $M\hat{g}$, and

an external driving force $F(t)$, all parallel to the direction of the inclined motion, the x-axis. It is evident that the total of the normal surface tractions exerted on the load M by the shear blocks is equipollent to zero. Clearly, other tractions that act on the shear blocks to control their simple shear deformation are of no concern here.

Let $x(t)$ denote the uniaxial motion of the center of mass of the load M relative to the undeformed position of the shear blocks, and note from Figure 1 that $\tan\alpha = x/L$. Then the equation of motion of the load is given by

$$ML\ddot{\sigma} = M\hat{g} + F(t) - 2AT_{12}(\sigma, \dot{\sigma}) \tag{2.1}$$

where $\hat{g} = g\sin\theta$. The shear stress $T_{12}(\sigma, \dot{\sigma})$ is considered next.

2.1. Shear stress for isotropic viscohyperelastic shear mounts

The shear stress relation in a simple shear deformation of a compressible or an incompressible, homogeneous and isotropic viscohyperelastic material introduced by Beatty and Zhou in [11] is given by

$$T_{12}(\sigma, \dot{\sigma}) = \sigma G(\sigma^2) + h\dot{\sigma}\ , \tag{2.2}$$

where the shear response function $G(\sigma^2)$ is a positive, even function of σ for which $G(0) \equiv G_0$ is the shear modulus in the natural state, and h is a constant viscosity coefficient. When $h = 0$, (2.2) yields the familiar constitutive equation for the shear stress in a compressible or incompressible, isotropic elastic solid [14]. Note that the shear stress is always an odd function of the amount of shear, so it acts on the shear mount in the direction of the shear; and hence an equal and oppositely directed restoring shear force acts on the load, as shown in Figure 1.

In particular, for the viscoelastic Mooney–Rivlin and neo-Hookean material models the shear response function is a positive constant, $G(\sigma^2) = G_0$; and hence for these models the shear stress in a simple shear deformation is given by the linear function $T_{12}(\sigma, \dot{\sigma}) = G_0\sigma + h\dot{\sigma}$. For other kinds of compressible and incompressible, homogeneous and isotropic hyperelastic materials studied in [5], the shear-response function is a quadratic function of the amount of shear:

$$G(\sigma^2) = G_0(1 + \varepsilon\sigma^2)\ , \tag{2.3}$$

where $G(0) = G_0 > 0$ and $\varepsilon \geq 0$. When $\varepsilon = 0$, we recover our previous linear models. Moreover, for rubberlike materials with a small second order modulus $\varepsilon \ll 1$, the relation (2.3) describes the 'roughly linear' shear stress response of simple shear springs mentioned earlier [1,2]. In this case, the nonlinear variation of the elastic shear-response function with the amount shear may be small, but it clearly is not ignorable for increasingly larger amounts of shear, a great fraction of which may arise from static deflection.

2.2. Formulation of the equations of motion

The equation of motion for the shear suspension system is now obtained by use of (2.2) and (2.3) in (2.1). Writing $F(t) = F_0\cos qt$, where F_0 and q are the maximum force intensity and the driving frequency, respectively, and introducing the dimensionless time variable $\tau \equiv \omega t$, we obtain the following dimensionless form of the equation of motion for the shear suspension system:

$$\sigma'' + 2\nu\sigma' + \sigma + \varepsilon\sigma^3 = \sigma_e(1 + \varepsilon\sigma_e^2) + \bar{Q}\cos\omega_f\tau\,. \tag{2.4}$$

Here the prime denotes the derivative with respect to τ, σ_e is the amount of static shear deflection of the load,

$$2\nu \equiv \frac{2A}{ML\omega}h, \quad \bar{Q} \equiv \frac{Q_0}{\omega^2}, \quad \omega_f \equiv \frac{q}{\omega}\,, \tag{2.5}$$

and

$$\omega^2 \equiv \frac{2A}{ML}G_0, \quad Q_0 \equiv \frac{F_0}{ML}\,. \tag{2.6}$$

Also, the equilibrium equation $2AT_{12}(\sigma_e, 0) = M\hat{g}$ for the load may be written as

$$\sigma_e(1 + \varepsilon\sigma_e^2) = \frac{p_0^2}{\omega^2}, \quad p_0^2 \equiv \frac{\hat{g}}{L}\,. \tag{2.7}$$

In a horizontal motion of the system, $\hat{g} = 0$ and $(2.7)_1$ yields $\sigma_e = 0$.

Solutions for the undamped and damped, free vibration of the load for which $\bar{Q} \equiv 0$ in (2.4) may be found in [11, 12]. Otherwise, (2.4) is a damped, forced Duffing equation with a constant equilibrium shift term that depends on ε and which cannot be removed by transformation. The solution of (2.4) has not been previously explored in the present physical context.

3. Analysis of the damped vibrational motion

Next we explore the finite-amplitude, damped vibrational motion of a load supported by compressible or incompressible, isotropic, viscohyperelastic shear mountings by studying the solution of the nonlinear equation (2.4). First, we sketch briefly the reduced form of (2.4) for damped, forced vibrations of the load on shear mountings having a constant shear-response function, and then recall the approximate solution for damped, free vibrations on shear mountings having a quadratic shear response function. We shall then study the steady-state, damped, forced vibrational motion of the load for the class of materials having quadratic shear response characterized by a small second-order modulus so that $0 < \varepsilon \ll 1$, and obtain the approximate solution of (2.4) by use of the method of harmonic balance. The physical behavior of the shear suspension system is then described both analytically and graphically.

3.1. Damped, forced vibration with constant shear response

Let us consider the class of viscohyperelastic materials characterized by a constant response function $G(\sigma^2) = G_0$ in (2.3). We thus set $\varepsilon = 0$ in (2.4) to obtain the governing equation for the damped, forced vibrational motion,

$$\sigma'' + 2\nu\sigma' + \sigma = \sigma_e + \bar{Q}\cos\omega_f\tau\,. \tag{3.1}$$

This equation is valid for the class of viscoelastic Mooney–Rivlin materials, for example. The ultimate equilibrium shear deformation σ_e is given by $(2.7)_1$. This is the ultimate amount of shear in a quasi-static creep due to gravity according to the solutions given by Beatty and Zhou [11]. If we transform (3.1) relative to σ_e by using $s = \sigma - \sigma_e$, then (3.1) becomes

$$s'' + 2\nu s' + s = \bar{Q}\cos\omega_f\tau\ . \tag{3.2}$$

Clearly, the nature of the solution of (3.2) is well-known and need not be discussed here. We note, however, that the steady-state solution of (3.2) for the *damped, forced vibrational motion* has the form

$$s(\tau) = \sigma(\tau) - \sigma_e = B\cos(\omega_f\tau - \phi)\ , \tag{3.3}$$

in which the amplitude B and initial phase ϕ depend on both the excitation frequency ω_f and the damping parameter ν.

3.2. Damped, free vibration with quadratic shear response

For viscohyperelastic materials having quadratic shear response, we return to the general equation of motion (2.4). For the damped, free vibrational motion, Beatty and Zhou [12] provide an approximate solution of (2.4) by the Kryloff-Bogoliuboff averaging method of slowly varying amplitude and phase [15]. Cast in terms of the notation used here, their solution for the *damped, free vibrational motion* may be written as

$$\sigma = \sigma_e + A_0 e^{-\nu\tau}\sin\left[\tau\left(1 + \frac{3}{2}\varepsilon\sigma_e^2\right) - \frac{3\varepsilon A_0^2}{16\nu}e^{-2\nu\tau} + \phi_0\right], \tag{3.4}$$

where A_0 and ϕ_0 are constants of integration that may be found from the assigned initial conditions as demonstrated in [12]. Otherwise, the solution of (2.4) for the damped, forced vibration case has not been explored in the present context. This is a nonlinear ordinary differential equation whose exact solution is unknown. In consequence, we shall seek its approximate steady-state solution.

3.3. Steady-state, damped vibration with quadratic shear response

To study the forced inclined motion of the load, we adopt the method of harmonic balance [15–19]. Accordingly, we recall (3.2) for the linear model and thus assume a steady-state solution of (2.4) of the familiar form (3.3):

$$\sigma = B\cos(\omega_f\tau - \phi) + c = a\sin\omega_f\tau + b\cos\omega_f\tau + c\ . \tag{3.5}$$

The constant c is introduced to account for the nonlinear equilibrium shift in (2.4), B denotes the constant, symmetric amplitude relative to the coordinate $\chi = \sigma - c$, and ϕ is the constant phase angle between the amplitude shear response B and the external driving force $\bar{Q}$. As usual,

$$a \equiv B\sin\phi, \quad b \equiv B\cos\phi\ , \tag{3.6}$$

and hence

$$B^2 = a^2 + b^2, \quad \tan\phi = \frac{a}{b}\ . \tag{3.7}$$

Clearly, both B and ϕ will depend strongly on the system parameters. Substituting (3.5) into (2.4) and applying the method of harmonic balance, we obtain the equilibrium shift equation

$$c\left(1+\frac{3\varepsilon B^2}{2}\right)+\varepsilon c^3=\sigma_e(1+\varepsilon\sigma_e^2)\ , \tag{3.8}$$

and the motion amplitude-excitation frequency response equation for an assigned driving force intensity $\bar{Q}$:

$$\omega_f^4+\omega_f^2[-\tfrac{3}{2}\varepsilon B^2-2(1-2\nu^2+3\varepsilon c^2)]+(1+3\varepsilon c^2)^2+\tfrac{3}{2}B^2\varepsilon\times$$

$$\times(1+3\varepsilon c^2+\tfrac{3}{8}\varepsilon B^2)-\frac{\bar{Q}^2}{B^2}=0\ . \tag{3.9}$$

The phase angle ϕ is given by

$$\phi=-\arctan\frac{2\nu\omega_f}{\omega_f^2-1-3\varepsilon c^2-\frac{3}{4}\varepsilon B^2}\ . \tag{3.10}$$

Notice that $c=\sigma_e$ if and only if $\varepsilon=0$, *i.e.* when and only when the shear-response function (2.3) is constant. Hence, clearly, the motion is asymmetric to the static equilibrium position at σ_e, whose value may be obtained from $(2.7)_1$. When B is prescribed, (3.9) is a quadratic equation in ω_f^2 whose exact solution is given by

$$\omega_f^2=-2\nu^2+\tfrac{3}{4}\varepsilon B^2+1+3\varepsilon c^2\pm\sqrt{4\nu^2[\nu^2-(1+3\varepsilon c^2+\tfrac{3}{4}\varepsilon B^2)]+\frac{\bar{Q}^2}{B^2}}\ , \tag{3.11}$$

and hence ϕ is determined by (3.10). Henceforward, we shall refer to the motion amplitude B as simply the amplitude, not to be confused with the driving-force amplitude $\bar{Q}$; and the excitation frequency ω_f will be called briefly the frequency, not to be confused with the system frequency ω. Therefore, (3.11) and any of its variants is called the amplitude-frequency equation.

Although (3.8) may be solved exactly for c, this inessential complication can be circumvented by use of its perturbation in the small parameter ε, as shown in [10]. We thereby obtain the approximate solution

$$c=\sigma_e(1-\tfrac{3}{2}B^2\varepsilon)\ . \tag{3.12}$$

We note that the estimate (3.12) is valid so long as $B<\sqrt{2/(3\varepsilon)}$, and hence the ultimate amplitude $B_c(\varepsilon)$ imposed by a positive shift c is given by

$$B_c(\varepsilon)=\sqrt{2/(3\varepsilon)}\ . \tag{3.13}$$

For small ε, this imposes no significant amplitude restriction. Using (3.12) in (3.11) and neglecting small terms $O(\varepsilon^2)$, we find

$$\omega_f^2=-2\nu^2+\frac{3}{4}\varepsilon B^2+\Omega^2\pm\sqrt{4\nu^2[\nu^2-(\Omega^2+\tfrac{3}{4}\varepsilon B^2)]+\frac{\bar{Q}^2}{B^2}}\ , \tag{3.14}$$

where, by definition,

$$\Omega^2 \equiv 1 + 3\varepsilon\sigma_e^2 \,. \tag{3.15}$$

We recall from [6] that Ω is the circular frequency for small amplitude, free vibrations of the load about its static state. Similarly, use of (3.12) in (3.10) yields the initial phase

$$\phi = -\tan^{-1}\left(\frac{2\nu\omega_f}{\omega_f^2 - \Omega^2 - \frac{3}{4}\varepsilon B^2}\right) \,. \tag{3.16}$$

With the results (3.14) and (3.16) in hand, the approximate steady-state solution (3.5) of Equation (2.4) now has the form

$$\sigma = \sigma_e(1 - \tfrac{3}{2}\varepsilon B^2) + B\cos(\omega_f\tau - \phi) \,. \tag{3.17}$$

4. Numerical solution and physical results

To conclude study of (3.17), we need to examine the amplitude-frequency response and other physical attributes of the system. As usual, we consider B as prescribed and $\omega_f(B)$ to be found, but its map is plotted as $|B|$ versus ω_f. First, we recall that the familiar parabolic-shaped backbone curve that describes the special undamped, free vibrational motion of the load is obtained from (3.14) when $\bar{Q}$ and ν vanish, namely,

$$|B| = \sqrt{\frac{4}{3\varepsilon}(\omega_f^2 - \Omega^2)} \,. \tag{4.1}$$

The plot of this function intersects the ω_f-axis at $\omega_f = \Omega$. In particular, for the horizontal motion, we set $\sigma_e = 0$ in (3.15) to obtain $\Omega = 1$, in which case the backbone curve (4.1) intersects the axis at $\omega_f = 1$. The shift of ω_f away from $\omega_f = 1$ is thus due to the gravitational effect in (2.7). Otherwise, the amplitude-frequency response for the horizontal motion is similar to that for the inclined motion, so we shall not consider it further.

For a fixed value of the ratio p_0/ω in the equilibrium equation $(2.7)_1$, that is, for the same load and shear spring characteristics, we may compute exactly the corresponding unique, positive equilibrium shear σ_e. To avoid this inessential complication, we adopt the first order perturbation estimate for σ_e given by

$$\sigma_e = r^2(1 - \varepsilon r^4) \quad \text{with} \quad r \equiv \frac{p_0}{\omega} \,. \tag{4.2}$$

Of course, for positive σ_e, we must have $r < \varepsilon^{-1/4}$, which for small ε clearly imposes no significant limitation. Otherwise, for each choice of r, ε, and a specified force intensity $\bar{Q}$, the amplitude-frequency response curves for small damping ν may be obtained from (3.14).

The effects of small damping in the amplitude-frequency response are illustrated in Figure 2 for selected parameters noted there. The ultimate amplitude (3.13) imposed by a positive static shift has been taken into account, and we have chosen $r^2 = \frac{1}{2}$ for the system design. For $\varepsilon = \{0{\cdot}02, 0{\cdot}04\}$ in the example shown here, (3.13) requires $B_c = \{5{\cdot}77, 4{\cdot}08\}$, respectively. Because of damping, the amplitude-frequency response curve cuts the backbone curve at a finite driving frequency, and the peak amplitude is finite. A sudden decrease (downward jump to E_1) in the amplitude of the motion occurs as the excitation frequency reaches point E

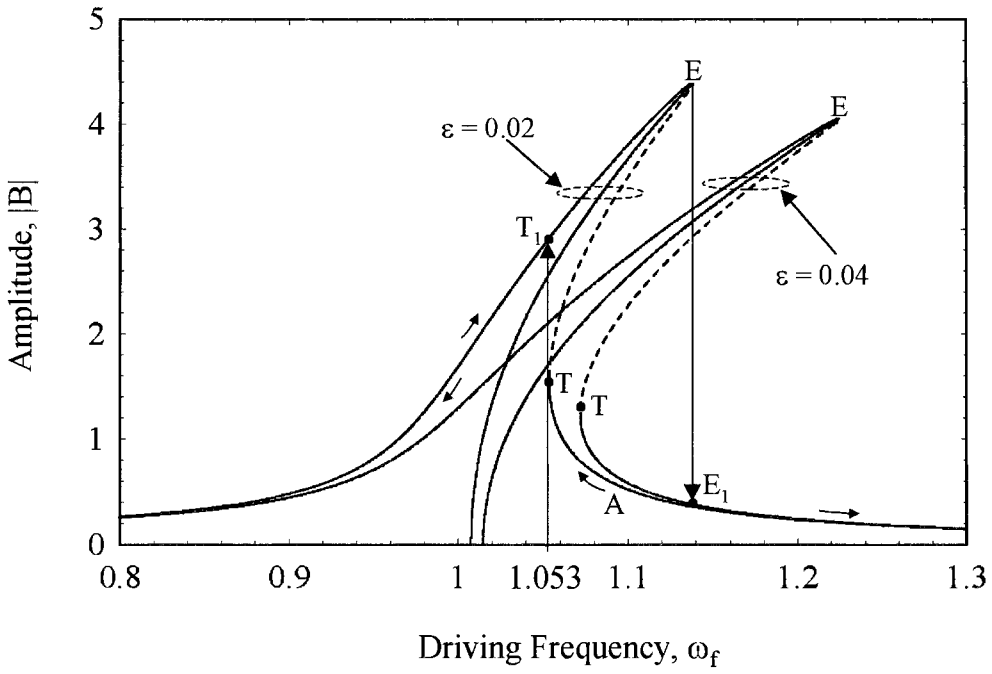

Figure 2. Amplitude-frequency response curves for the inclined damped motion of the load for values of $(\varepsilon, \sigma_e) =$ (0·02, 0·497), (0·04,0·495), $\bar{Q} = 0{\cdot}1$, and $\nu = 0{\cdot}01$, when $r = \sqrt{2}/2$.

in Figure 2. And when the frequency is gradually decreased from a higher value, a sudden increase (upward jump to T_1) in the amplitude occurs at point T in Figure 2. The points E and T thus represent the limit between stable and unstable motions. The dashed lines between these bifurcation points emphasize unstable states that are unattainable. The bifurcation point T plainly occurs at the vertical tangent. We shall return to this later.

Use of (4.1) in (3.16) shows that the phase angle at the bifurcation point E in Figure 2 has the universal value $\phi = -\pi/2$. This phenomenon is described in Figure 3 for the same parameter set used in the plots for Figure 2. It is seen from Figures 2 and 3 that, as the frequency ω_f increases from zero, the amplitude response of the system for $-\pi/2 < \phi \leq 0$ is in phase with the driving force until the response reaches E where $\phi = -\pi/2$. For any further increase in the frequency, the point E jumps suddenly from E to E_1 in Figures 2 and 3; and the motion response and excitation force are now out of phase for $-\pi \leq \phi < -\pi/2$. After the point moves from E_1 for increasing values of ω_f, the amplitude of the oscillations decreases and the response continues out of phase with the excitation. If the system is operating at a high value of ω_f, say at point A in Figure 3, the response is out of phase with the excitation; and as the driving frequency ω_f is decreased, the response moves from A to T in Figures 2 and 3. The motion jumps suddenly from T to T_1 for any further decrease in the value of ω_f. This results in a large increase in the amplitude of oscillations of the load, and the response is again in phase with the excitation. After the response moves from T_1 for decreasing values of ω_f, the amplitude of oscillation decreases as well, and the response continues in phase with the driving force.

The results exhibited in Figures 2 and 3 characterize the general motion of the system for any selected set of system design parameters. To complete the physical description of the

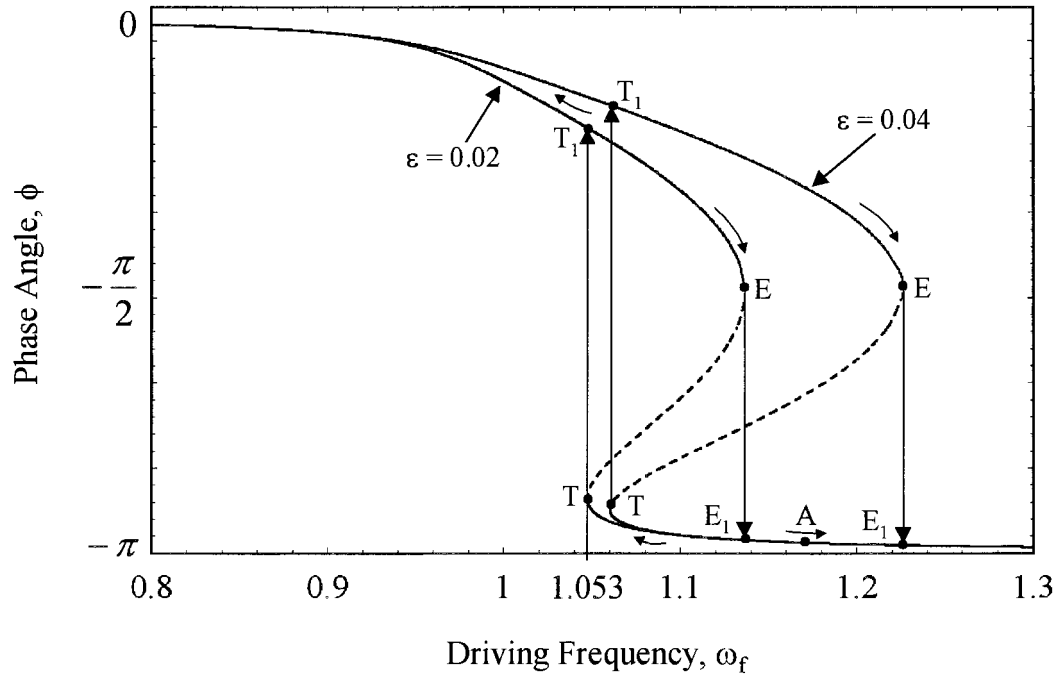

Figure 3. Phase angle-frequency plots for the inclined damped motion of the load for the same parameter values illustrated in Figure 2.

motion, however, we need to determine the bifurcation conditions and examine the stability of the system.

4.1. Bifurcation conditions

To find the bifurcation points of the motion, we rewrite (3.14) and introduce the transformation $y = B^2$ to obtain

$$y^3 + a_2 y^2 + a_1 y + a_0 = 0\,, \tag{4.3}$$

where

$$a_0 = -\frac{16\bar{Q}^2}{9\varepsilon^2}, \quad a_1 = \frac{16}{9\varepsilon^2}[(\omega_f^2 - \Omega^2)^2 + 4\nu^2\omega_f^2], \quad a_2 = \frac{8}{3\varepsilon}(\Omega^2 - \omega_f^2)\,. \tag{4.4}$$

The number of real roots of (4.3) is determined by its discriminant

$$D \equiv q^{*3} + r^{*2}\,, \tag{4.5}$$

where

$$q^* = \frac{a_1}{3} - \frac{a_2^2}{9}, \quad r^* = \tfrac{1}{6}(a_1 a_2 - 3a_0) - \tfrac{1}{27}a_2^3\,. \tag{4.6}$$

In general, if $D > 0$, there is only one real root of (4.3); if $D = 0$, there are three roots at least two of which are equal; and if $D < 0$, there are three distinct, real roots. The bifurcation

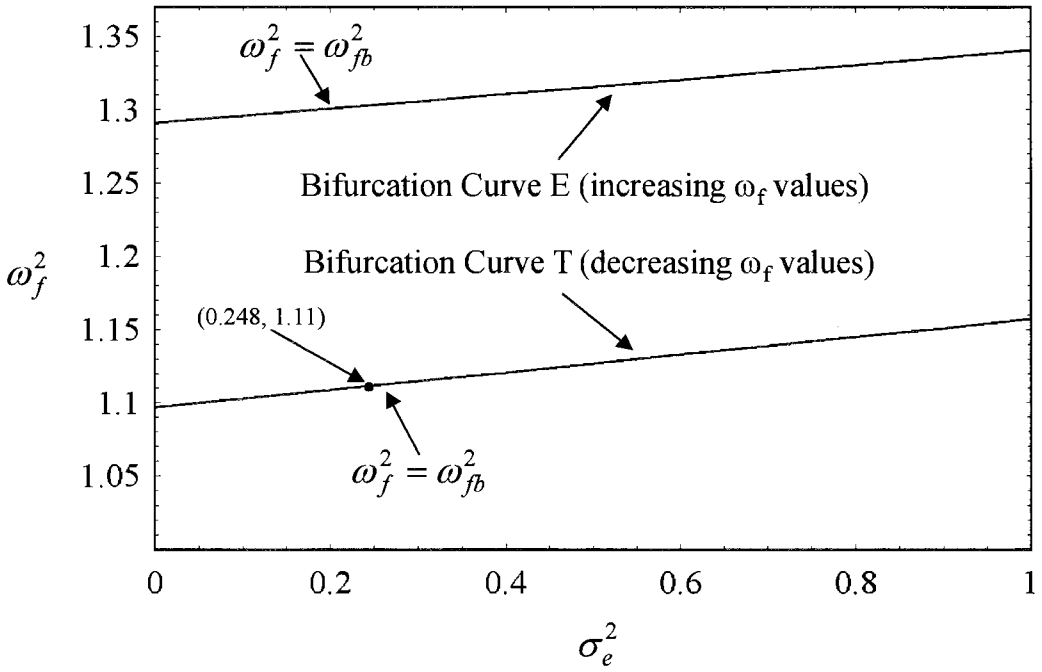

Figure 4. Plot of ω_{fb}^2 versus σ_e^2 at which the damped motion bifurcates for $\varepsilon = 0.02$, $\bar{Q}$ =0·1, and ν =0·01. The point (0·248, 1·11) corresponds to values (σ_e, ω_{fb}) =(0·497, 1·053).

frequency occurs at values $\omega_f = \omega_{fb}$ for which $D = 0$; and hence, this condition will aid in our identifying design-parameter values that control the motion and stability of the system.

Now consider the physical situation. Since $y = B^2 > 0$, we know that physically meaningful roots of (4.3) must be positive. Notice that $a_0 < 0$ and $a_1 > 0$. Therefore, in accordance with Descartes's rule of signs, (4.3) may have three positive real roots if and only if $a_2 < 0$; hence, by $(4.4)_3$, when and only when $\omega_f^2 > \Omega^2$. At a bifurcation frequency $\omega_f = \omega_{fb}$, two of these roots are identical; otherwise, one of the three distinct positive roots of (4.3) is inherently unstable and unattainable. When $\omega_f^2 = \Omega^2$, $a_2 = 0$; and hence (4.5) shows that $D > 0$. Clearly, if $a_2 > 0$, (4.3) has at most one positive real root of physical interest; and any negative real roots lack physical content and may be ignored. Therefore, no bifurcation or inherent instability occurs for any excitation frequency $\omega_f^2 \leq \Omega^2$; bifurcation and instability can occur only for certain operating frequencies $\omega_f^2 > \Omega^2$ for which $D = 0$.

We recall that ε is a specified small material parameter; and the amount of static shear deflection of the load σ_e is determined by the system design and load intensity in accordance with (2.7). Therefore, Ω defined in (3.15) is an inclusive system design parameter. Let Ω_d denote a specified value for the system design parameter Ω. Then, in accordance with our previous argument, the safe operating design criterion for which no bifurcation or inherent instability will arise is provided by

$$\omega_f^2 \leq \Omega_d^2 \,. \tag{4.7}$$

For an assigned value of ε, the relation (3.15) in a plot of Ω_d^2 versus σ_e^2 shows that operating speeds situated on or below the straight line $\Omega_d^2 = 1 + 3\varepsilon\sigma_e^2$ are safe. This does not preclude existence of a safe operating frequency for which $\omega_f^2 > \Omega_d^2$, provided ω_f is not a bifurcation

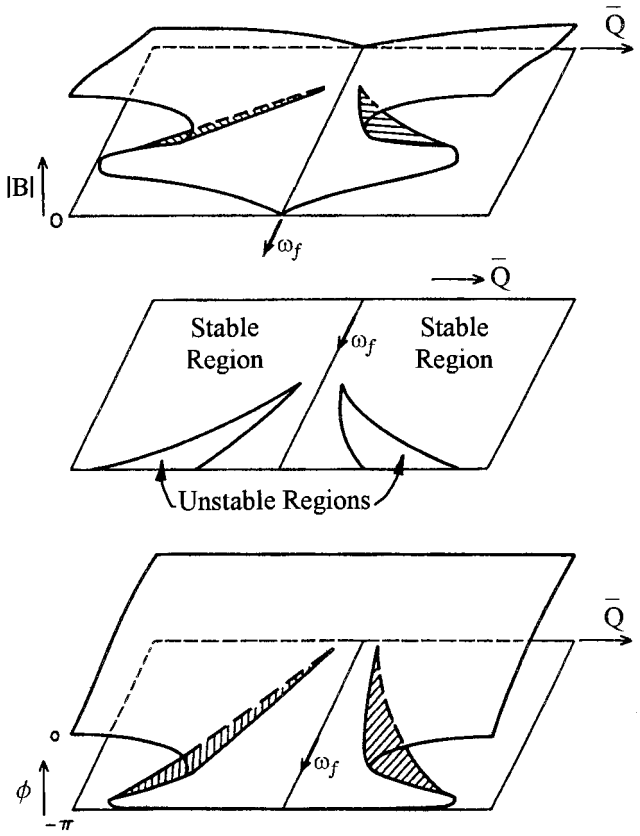

Figure 5. Schematic of the solution surface in $(\omega_f, \bar{Q}, |B|)$-space shown in the upper diagram, its view from above shown in the central diagram, and the solution surface in $(\omega_f, \bar{Q}, \phi)$-space shown in the lower diagram, all for the same specified values of the parameter set $(\varepsilon, \sigma_e, \nu)$. (Adapted from [13].

frequency for which $D = 0$. For the examples in Figures 2 and 3, we find $\omega_f \leq \Omega_d =$(1·007, 1.015). Hence, we see clearly in these sample illustrations that (4.7) indeed yields a safe value for the operating frequency; and higher, safe operating frequencies exist, except at the bifurcation points E and T.

Let ω_{fb} denote the driving frequency at a bifurcation point for which $D = 0$ in (4.5), namely,

$$\frac{8\vartheta_c}{81\varepsilon}\left[\omega_{fb}^2 - \Omega_d^2 \pm \sqrt{\vartheta_c}\right] = \bar{Q}^2 \tag{4.8}$$

where, by definition,

$$\vartheta_c \equiv (\Omega_d^2 - \omega_{fb}^2)^2 - 12\nu^2\omega_{fb}^2 \,. \tag{4.9}$$

For a given viscohyperelastic shear-spring material with small damping ν and quadratic shear response, with a specified design value for the driving-force intensity $\bar{Q}$ and a design parameter value Ω_d^2 defined by (3.15), two bifurcation values ω_{fb}^2 of the excitation frequency are determined by (4.8). These correspond to points T and E in Figures 2 and 3. For design-illustration purposes, let us consider the variation of ω_{fb}^2 versus σ_e^2 shown in Figure 4, for

fixed material values $\varepsilon = 0{\cdot}02$, $\nu = 0{\cdot}01$, and an excitation amplitude $\bar{Q} = 0{\cdot}1$. We thus obtain from (4.8) two bifurcation curves $\omega_f^2 = \omega_{fb}^2$ in Figure 4 that are the loci of bifurcation points T and E belonging to the corresponding family of amplitude-frequency response curves. For any specified system design, the bifurcation points and a safe system operating range may be read from the design plots in Figure 4. (While these plots have the appearance of straight lines over the range of values shown here, they actually are curved.) In this way, for any specified system-parameter design values of ε, σ_e, $\bar{Q}$, and ν, a suitable excitation frequency operating range can be decided for which the motion will be stable, for example. Conversely, for any specified excitation frequency, (4.8) may be applied to determine various critical design-parameter values. The utility of our simple bifurcation maps in Figure 4 applied to any typical system design is underscored by the stability analysis presented farther on.

For specified values of ε, σ_e, ν, our solution set forms a three-dimensional surface in $(\omega_f, \bar{Q}, |B|)$-space shown schematically in the upper diagram of Figure 5, which is based on the general analysis due to Holmes and Rand [13]. Here we illustrate its relation to the physical problem of nonlinear shearing vibrations with damping. A cross-section through this surface defined by the plane $\omega_f = 1{\cdot}2$ in Figure 6 shows the relationship between $\bar{Q}$ and $|B|$ for a few fixed values of the parameter set ε, σ_e, ν. Due to the presence of small damping, the curves in Figure 6 do not intersect the vertical line at the points $\bar{Q} = 0$, a characteristic of the undamped case studied in [10]. The three-dimensional schematic in Figure 5 provides an overview of the general physical characteristics represented in the special plane map of Figure 6. We shall say more about this in a moment. As one expects, Figure 6 shows that large excitation forces produce large-amplitude vibrations of the load, and if one starts with either a sufficiently small or large excitation force, no amplitude jumps can occur. Here we note that the curves marked as $|B < 0|$ and $|B > 0|$ in Figure 6, and farther on in Figure 9, are maps for which the amplitude $B < 0$ and $B > 0$, respectively, are plotted as $|B|$. We recall that the motion for $B < 0$ is out of phase with the driving force.

Now return to (4.5) and let $\bar{Q}_J$ denote the value of the driving-force intensity at a bifurcation frequency ω_{fb} for which $D = 0$. We obtain equations that are similar to and which may be read directly from those in (4.8) and (4.9). For a given set of design parameters ε, σ_e, ν, we thus determine the bifurcation values of the driving-force amplitude $\bar{Q}_J(\omega_{fb})$ as a function of the corresponding excitation frequency ω_{fb}. This bifurcation diagram is plotted in Figure 7 for two values of the second-order shear modulus ε and in Figure 8 for two values of the damping coefficient ν. The stability boundaries in Figures 7 and 8 are the curves for which $|\bar{Q}| = \bar{Q}_J$ and $\omega_f = \omega_{fb}$, *i.e.* $\bar{Q}_J(\omega_{fb})$. The characteristic cusp shape and symmetry about $\bar{Q} = 0$ is evident [13]. Notice also that the cusps do not converge at the origin as they do for the undamped case; and when small forces act on the system the solutions do not bifurcate; we see again the safe region defined by (4.7). The bifurcation points T and E of the amplitude-frequency curves in the example of Figure 2 are on the stability boundary of the bifurcation curves in Figures 7 and 8. The points T and E in Figure 2 correspond, respectively, to the bifurcation points J and H in Figure 6. The plots in Figures 7 and 8 are essentially different views of the same solution surface shown schematically in Figure 5 and viewed from above, as illustrated schematically in the central diagram of Figure 5. The phase-angle-frequency diagram in Figure 3 corresponds to a cross-section by the plane $\bar{Q} = 0{\cdot}1$ through the solution surface shown in the lower schematic diagram of Figure 5. The criterion (4.7) for a safe operating frequency is evident in all of these stability diagrams. The general overall safe operating range is provided by the simple stability map in Figure 4; this

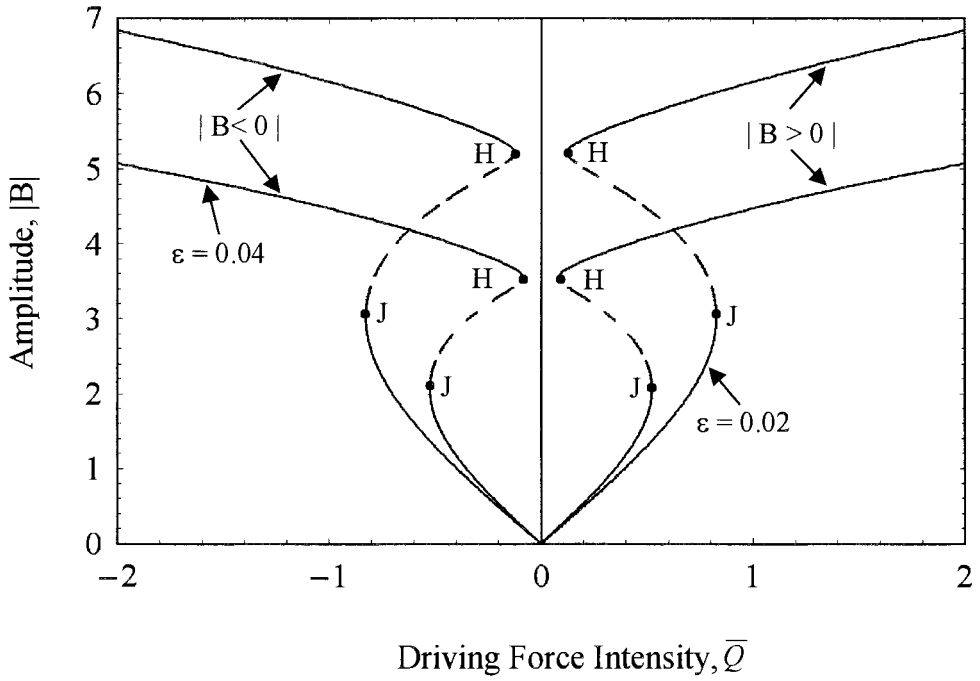

Figure 6. Motion amplitude-driving force amplitude curves for (ε, σ_e) =(0·02, 0·497), (0·04, 0·495), ν =0·01, and ω_f =1·2. The latter defines a plane section through the solution surface shown schematically in the top diagram of Figure 5.

characterizes the stability of the forced damped, inclined motion of the system for specified parameter values.

4.2. INFINITESIMAL STABILITY OF THE MOTION

In previous discussions, we have argued intuitively that the dotted portion TE of the amplitude-frequency response curve shown in Figure 2, and hence throughout our subsequent description, represents inherently unstable, unattainable states of the motion. In this section, we reinforce this physical argument by briefly examining more closely the infinitesimal stability of the steady-state, forced vibrational motion $\sigma(\tau)$ of the load described by (2.4).

Let $\sigma(\tau)$ and $\hat{\sigma}(\tau) = \sigma(\tau) + w^*(\tau)$ denote two solutions of the equation of motion (2.4) for which the initial conditions for $\hat{\sigma}(\tau)$ and $\sigma(\tau)$ at $\tau = 0$ are very nearly the same. Substituting $\hat{\sigma}(\tau)$ for $\sigma(\tau)$ in (2.4), noting that $\sigma(\tau)$ satisfies the same equation, and neglecting powers of $w^*(\tau)$ greater than the first, we obtain the linearized equation for the small perturbed motion $w^*(\tau)$:

$$w^{*\prime\prime} + 2\nu w^{*\prime} + w^*(1 + 3\varepsilon\sigma^2) = 0\,. \tag{4.10}$$

We next introduce the transformation

$$w^*(\tau) = \mathrm{e}^{-\nu\tau} w(\tau) \tag{4.11}$$

to obtain from (4.10) the following linear differential equation with a time-dependent coefficient:

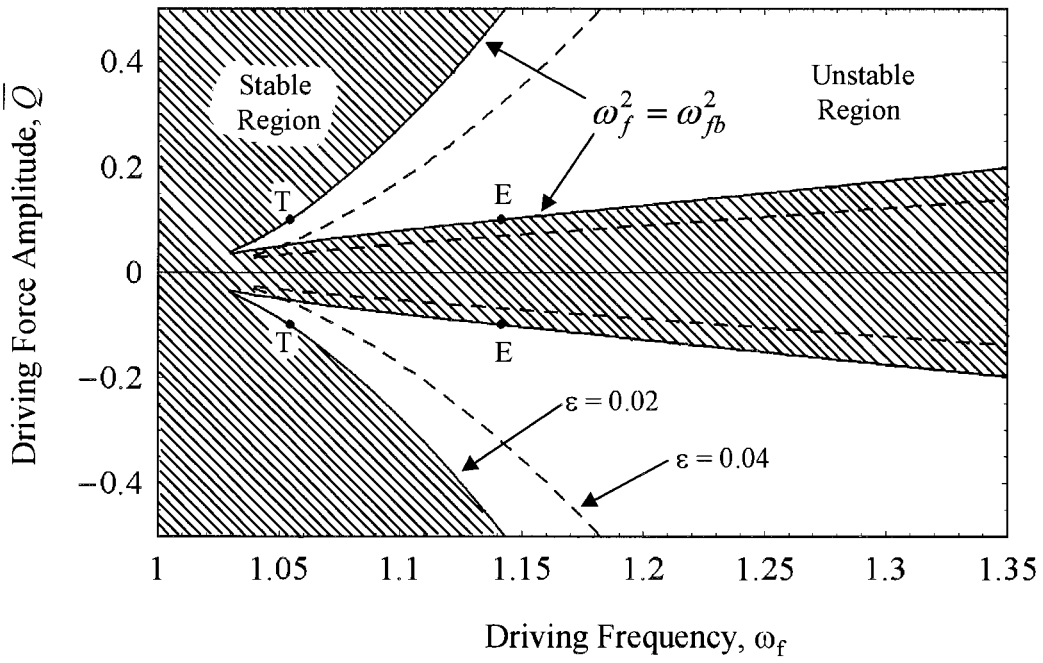

Figure 7. Bifurcation solutions in $\bar{Q} - \omega_f$ space for values of (ε, σ_e) =(0·02, 0·497), (0·04, 0·495) and a fixed damping value of ν =0·01. This is a top view of the solution surface as shown schematically in the central diagram of Figure 5.

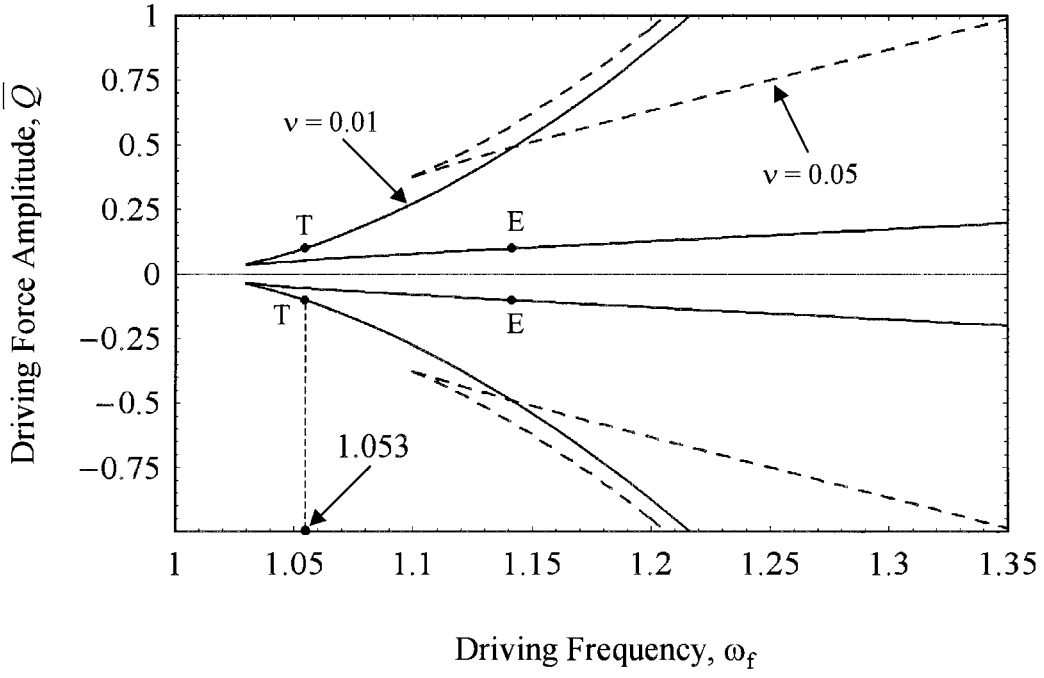

Figure 8. Bifurcation solutions in $\bar{Q}$-ω_f space for values of ν =0·01, 0·05 and a design pair (ε, σ_e) =(0·02, 0·497). This is an alternative top view of the solution surface as shown schematically in the central diagram of Figure5.

$$w'' + w(1 - \nu^2 + 3\varepsilon\sigma^2) = 0 \,. \tag{4.12}$$

If the solution $w(\tau)$ of this equation is bounded, the perturbed motion (4.11) decays and $\sigma(\tau)$ is said to be stable; otherwise, the motion $\sigma(\tau)$ is called unstable.

We consider the steady-state solution (3.5) and introduce $Z = \omega_f \tau - \phi$ as the new independent variable to write $\sigma = B\cos Z + c$ and $w'' = \omega_f^2 \mathrm{d}^2 w/\mathrm{d}Z^2$. Then (4.12) transforms to the three-parameter Hill equation:

$$\frac{\mathrm{d}^2 w}{\mathrm{d}Z^2} + w(d_1 + d_2\cos Z + d_3\cos 2Z) = 0 \,, \tag{4.13}$$

where

$$d_1 \equiv \frac{1}{\omega_f^2}(1 - \nu^2 + \frac{3}{2}\varepsilon B^2 + 3\varepsilon c^2), \quad d_2 \equiv \frac{6\varepsilon c B}{\omega_f^2}, \quad d_3 \equiv \frac{3\varepsilon B^2}{2\omega_f^2} \tag{4.14}$$

are constants. For this equation, approximate results and stability boundaries of the motion may be found in [20]–[23], for example. Notice in the derivation leading to (4.13) that all order terms in ε have been retained.

Equation (4.13) characterizes the perturbed inclined motion of the load on simple shear mounts. Notice that d_2 arises from the equilibrium shift c; and hence to simplify our concluding remarks, we first consider the horizontal case.

4.2.1. *Stability of the horizontal motion*

For a horizontal motion, $\sigma_e = 0$ and (3.8) shows that $c = 0$. In this case $d_2 = 0$ in (4.14); and (4.13) thus reduces to the standard Mathieu equation [17, pp. 202–219], namely,

$$\frac{\mathrm{d}^2 w}{\mathrm{d}y^2} + [\delta + \epsilon\cos y]w = 0 \,, \tag{4.15}$$

where $y \equiv 2Z$ and the constant coefficients are defined by

$$\delta \equiv \frac{d_1}{4} = \frac{1}{4\omega_f^2}(1 - \nu^2 + 4\omega_f^2\epsilon), \quad \epsilon \equiv \frac{d_3}{4} = \frac{3\varepsilon B^2}{8\omega_f^2} \,. \tag{4.16}$$

The commonly used Mathieu parameter ϵ defined in $(4.16)_2$ appears only in our discussion of stability graphs related to the Mathieu equation (4.15), so one should encounter no serious confusion with our physical parameter ε for which only numerical values used in earlier examples are noted in two places below.

Because ε is small, we shall assume that values of ϵ are small too. Hence, in accordance with [17, pp. 208–213], the transition curves for the stability boundaries in the $\delta - \epsilon$ plane for the Mathieu equation (4.15), up to terms of second order in ϵ^2, are given by

$$\delta = \frac{1}{4} \pm \frac{\epsilon}{2}, \quad \delta = -\frac{\epsilon^2}{2} \,. \tag{4.17}$$

The curves $\delta = \delta(\epsilon)$ define the boundary curves of the stable (shaded) regions of the Mathieu equation. Each point of these boundary curves corresponds to a periodic solution of (4.15) of period 2π or 4π. The common practice is to plot these curves as ϵ versus δ, as

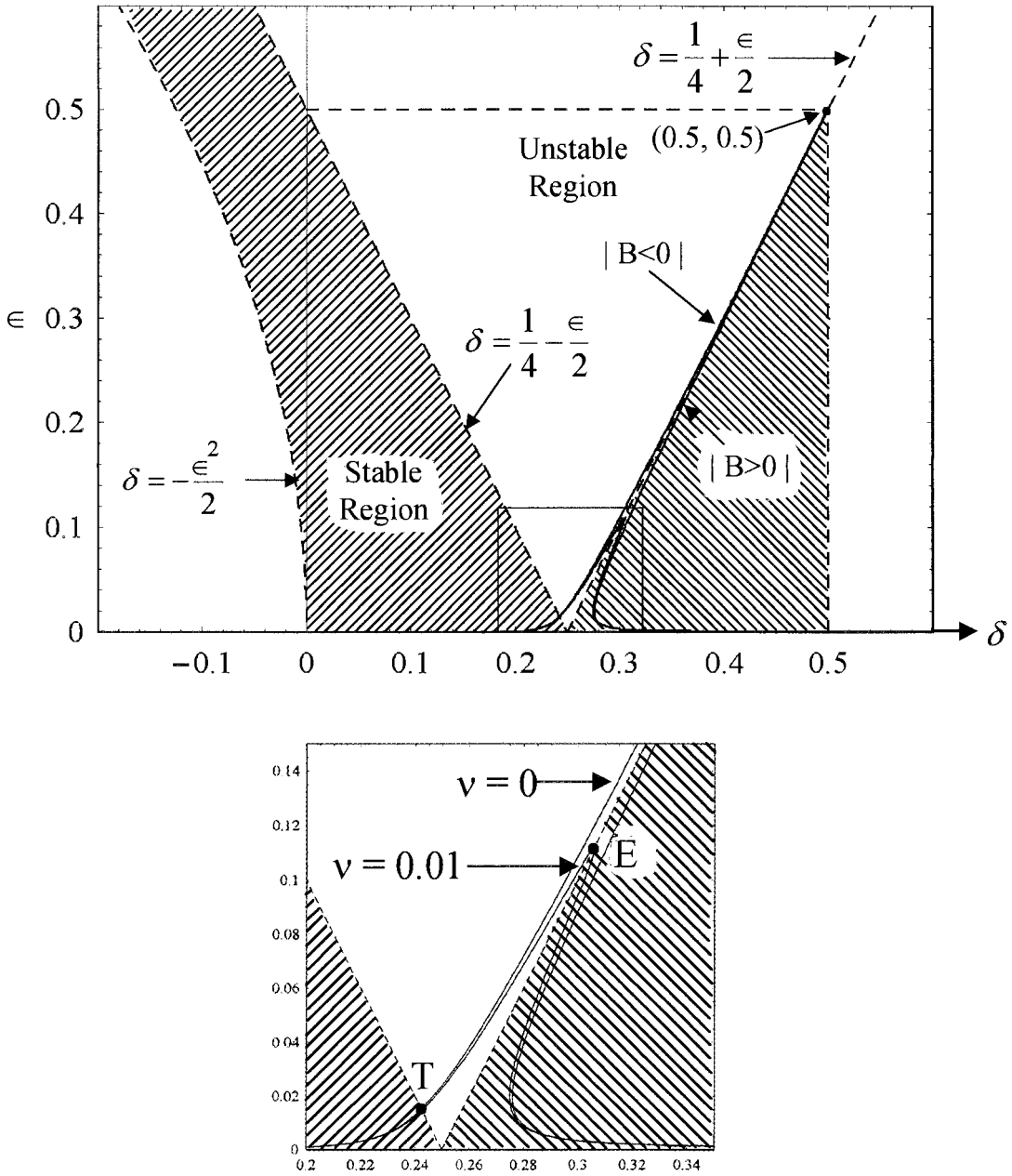

Figure 9. Stability curves of the Mathieu equation (dotted lines) and the shear mount system response curves (solid lines) for forced horizontal motion of the load.

shown in Figure 9. For the damped horizontal motion, the points T and E shown in Figure 9 correspond to the points T and E on the physical response curves similar to that shown in Figure 2. We thus confirm that these points lie on the Mathieu boundaries identified as $|B < 0|$, where we recall that the motion for $B < 0$ is out of phase with the driving force. It is known that these boundary lines represent the transition between stable and unstable solutions of the system. For details, see [17, pp. 213–219] for example. Specifically, we see from the magnified portion of the stability curves of Figure 9 that the point T of the physical response

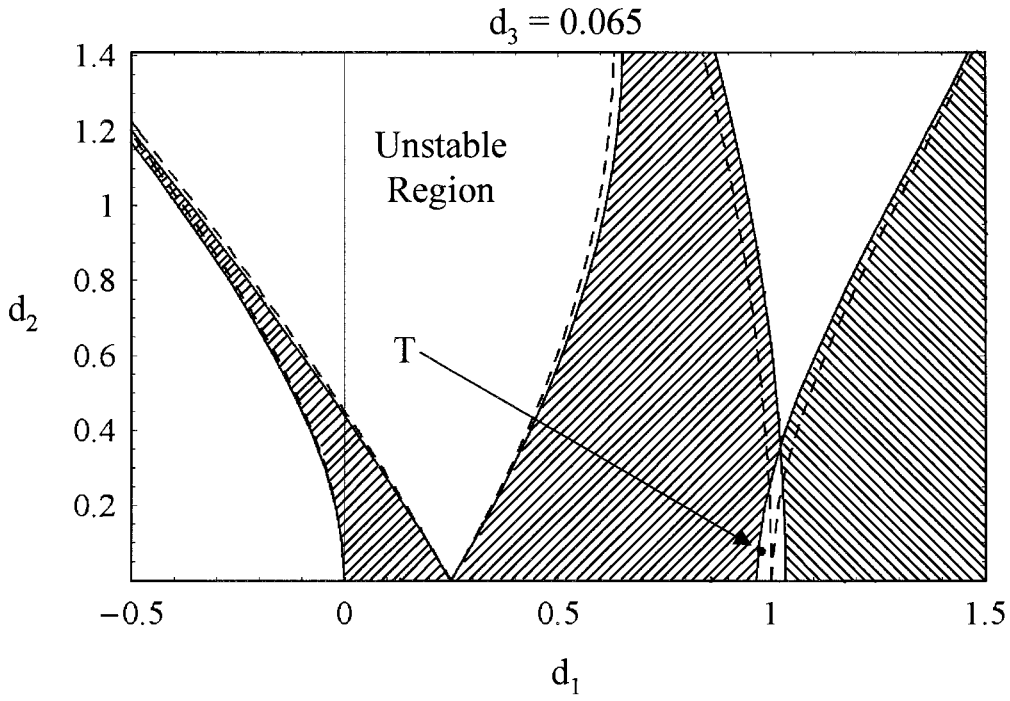

Figure 10. Stability maps of the three-parameter Hill equation for $d_3 = 0{\cdot}065$ (solid curves).

curve intersects the line $\delta = \frac{1}{4} - \epsilon/2$ while E intersects the line $\delta = \frac{1}{4} + \epsilon/2$. Hence, the physical response between the points T and E for $B < 0$ falls in the unstable region of the stability map in Figure 9, clearly indicating that the system is indeed unstable. Hence, the amplitude-frequency response curve TE for the horizontal motion, which is similar to the response shown in Figure 2 and subsequent figures for the inclined motion, defines inherently unstable, unattainable states of the motion, as described earlier.

4.2.2. *Stability of the inclined motion*

When the motion is inclined $d_2 \neq 0$ and now we have a more complicated analysis based on the three-parameter Hill equation. The determination of its stability conditions for the unstable regions may be found in several resources, [20]–[23] for example. As usual, the bifurcation points in the amplitude-frequency response curves in Figure 2 represent the transition between stable and unstable motions. To obtain stability maps similar to those for the Mathieu equation, we may use the approximate, Fourier series solution of (4.13) developed by Klotter and Kotowski [23]. The stability maps and their stability boundaries are thereby determined numerically for a specified value of d_3. We omit these details, refer the reader to [23], and illustrate in Figure 10 our stability maps for $d_3 = 0{\cdot}065$.

Because the stability maps depend on the values of d_1, d_2, and d_3, we need to know their behavior with respect to ω_f. Figure 11 shows the plots of d_1, $|d_2|$, and d_3 versus ω_f for our earlier example values of $(\varepsilon, \sigma_e) = (0{\cdot}02, 0{\cdot}497)$, $\nu = 0{\cdot}01$, and $\bar{Q} = 0{\cdot}1$. The corresponding values of ω_f, d_1, and d_2 for $d_3 = 0{\cdot}065$ are $1{\cdot}053$, $0{\cdot}977$, and $0{\cdot}077$, respectively. Notice that the three Hill parameters d_k have a common vertical tangent at the bifurcation frequency $\omega_f = \omega_{fb} = 1{\cdot}053$ in the example. These values are used to determine the stability of the motion from Figure 10. The solid lines in Figure 10 represent stability boundaries in the

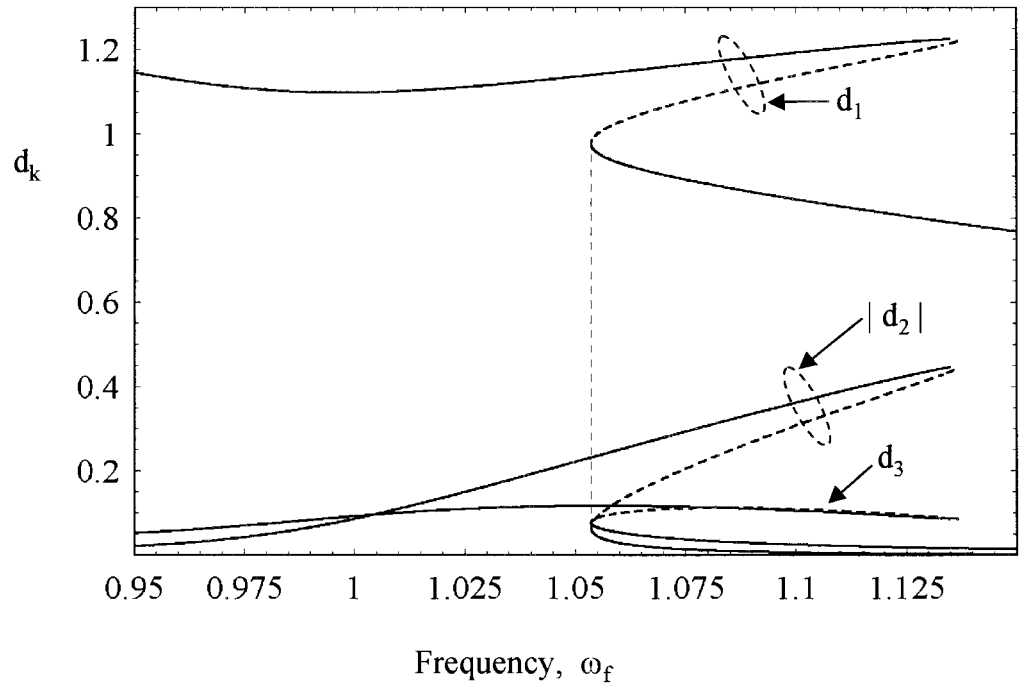

Figure 11. Variation of d_1, $|d_2|$, and d_3 versus ω_f for values of (ε, σ_e) =(0·02, 0·497), ν =0·01, and $\bar{Q}$ =0·1.

physical problem for which d_3 =0·065, and hence we are dealing here with the full three-parameter Hill equation. The dotted curves in Figure 10, however, are merely reference curves for the stability boundaries of the standard Mathieu equation for which $\delta = d_1$ and $\epsilon = d_2$. While this corresponds to formally setting $d_3 = 0$ in (4.13), it should be evident that for our physical problem $d_3 \neq 0$ in (4.14). With the above values and from Figure 10, it is found that the solution at the point T shown here is indeed unstable. The reader will observe that this result agrees with the plots presented in Figures 2, 3, 4, 7, and 8, in which the bifurcation point T occurs at an excitation frequency ω_f =1·053. These rather complicated procedures underscore the great simplicity of the representation of the loci of the bifurcation points provided in our simple stability diagram in Figure 4 giving the bifurcation frequency at both T and E for any specified design value σ_e.

5. Concluding remarks

We have studied the problem of the damped, finite-amplitude forced vibration of a load supported symmetrically by simple shear springs and by a smooth inclined bearing surface. The results obtained here are valid for all compressible or incompressible, homogeneous and isotropic, viscohyperelastic spring materials for which the shear response function in a simple shear deformation is a quadratic function of the amount of shear. This function models the finite displacement of shear mountings that may operate beyond, but close to the linear range of shear response observed in experiments. We find that even a small nonlinearity in the shear response can produce potentially undesirable dynamical effects on the motion, which is characterized by the forced Duffing equation with damping and with a constant static shift term due to gravity. An exact solution of this equation, even when gravity is absent, is unknown,

so we study its approximate solution by the classical method of harmonic balance. Because of the nonlinear nature of the equation of motion, the static shift factor cannot be transformed away. The physical relevance and complex effects of the static shift on the stability of the motion is emphasized throughout this study.

The system design parameters are related to the dynamical response of the system for small damping. Regions of stable motion are identified in terms of the amplitude of the motion, driving-force intensity, driving frequency, and system design-parameters. Bifurcation limits on the driving frequency for stable motion of the system are identified analytically and illustrated graphically in Figures 2 and 3. In consequence, a safe operating design criterion that guarantees stable motion of the load for any specified system design parameter values $(\varepsilon, \sigma_e, \bar{Q}, \nu)$ is derived; and the result is described graphically in Figure 4. This simple diagram maps the loci of all bifurcation points against the static shear deflection, which serves as the principal system design parameter for the inclined motion. In consequence, for any specified system design, the bifurcation points and a safe system operating range may be read from these design plots; and, hence, a suitable excitation frequency operating range can be decided for which the motion will be stable. Conversely, for any specified excitation frequency, various critical design parameter values may be determined. The effects of the driving-force intensity $\bar{Q}$ on the amplitude of the motion and on the range of stable motions for any assigned operating frequency, for selected material constants, are illustrated in Figures 6, 7 and 8. These maps provide alternative means of assessing overall safe operating conditions for the system. The utility and simplicity of our bifurcation maps in Figure 4 applied to any typical system design is underscored by our infinitesimal stability analysis of the system. This analysis shows that the bifurcation points of the inclined motion fall on the stability boundaries of the numerical solution of a complex, three-parameter Hill equation.

In short, the solution presented here provides information that illustrates how system design parameters affect the motion of the load and how these may be chosen to control the amplitude of the oscillations and the stability of the system. In future work, we shall build on this problem analysis to explore the controlling effect of a vibration absorber.

Acknowledgement

This work was partially funded by Grant No. CMS-9634817 from the National Science Foundation, with partial matching support provided by the University of Nebraska Center for Materials Research and Analysis.

References

1. J. F. Downie Smith, Rubber springs–shear loading. *J. Appl. Mech.* 61 (1939) A159–A167.
2. C. M. Harris and C. E. Crede, *Shock and Vibration Handbook, vol. 2. Data Analysis, Testing and Methods of Control*. New York: McGraw-Hill (1961) pp. 35.1–35.18.
3. P. K. Freakley and A. R. Payne, *Theory and Practice of Engineering with Rubber.* London: Applied Science (1978) 666 pp.
4. D. C. Allen, Use of rubber in shock packaging. In: P. W. Allen, P. B. Lindley and A. R. Payne (Eds.), *Use of Rubber in Engineering.* London: Maclaren (1967) pp. 220–230.
5. M. F. Beatty, Finite amplitude vibrations of a body supported by simple shear springs. *J Appl. Mech.* 106 (1984) 361–366.
6. M. F. Beatty, Finite amplitude, periodic motion of a body supported by arbitrary isotropic elastic shear mountings. *J. Elasticity* 20 (1988) 203–230.

7. M. F. Beatty, Stability of a body supported by a simple vehicular shear suspension system. *Int. J. Non-Linear Mech.* 24 (1989) 65–77.
8. M. F. Beatty and R. Bhattacharyya, Stability of the free vibrational motion of a vehicular body supported by rubber shear mountings with quadratic response. *Int. J. Non-Linear Mech.* 24 (1989) 401–414.
9. R. Bhattacharyya, Stability of the forced vibrational motion of a vehicular body supported by rubber shear mountings with quadratic response. *Int. J. Non-Linear Mech.* 24 (1989) 467–482.
10. A. E. Zúñiga and M. F. Beatty, Forced vibrations of a body supported by hyperelastic shear mountings. Submitted.
11. M. F. Beatty and Z. Zhou, Finite amplitude, free vibrations of a body supported by incompressible, nonlinear viscoelastic shear mountings. *Int. J. Solids Struct.* 27 (1991) 355–370.
12. M. F. Beatty and Z. Zhou, Simple shearing of an incompressible, viscoelastic quadratic material. *Int. J. Solids Strucs.* 23 (1994) 3201–3215.
13. P. J. Holmes and D. A. Rand, The bifurcation of Duffing's equation: An application of catastrophe theory. *J. Sound Vibr.* 44 (1976) 237–253.
14. M. F. Beatty, Introduction to nonlinear elasticity. In: M. M. Carroll and M. A. Hayes (eds), *Nonlinear Effects in Fluids and Solids.* New York and London: Plenum Press (1996) pp. 13–104.
15. J. A. Sanders and F. Verhulst, *Averaging Methods in Nonlinear Dynamical Systems.* New York: Springer-Verlag (1985) 247 pp.
16. A. H. Nayfeh and D. T. Mook, *Non-linear Oscillations.* New York: John Wiley (1973) 704 pp.
17. J. J. Stoker, *Non-linear Vibrations in Mechanical and Electrical Systems.* New York: Interscience (1950) 273 pp.
18. R. E. Mickens, Comments on the method of harmonic balance. *J. Sound Vibr.* 94 (1984) 456–460.
19. R. E. Mickens, A generalization of the method of harmonic balance. *J. Sound Vibr.* 111 (1986) 515–518.
20. B. Porter, The stability of systems governed by a special form of Hill's equation. *Int J. Mech Sci.* 4 (1962) 313–321.
21. K. Hamer and M. R. Smith, Stability of the general Hill's equation with three independent parameters. *J. Appl. Mech.* 39 (1972) 276–278.
22. L. A. Rubenfeld, The stability surfaces of a Hill's equation with several small parameters. *J. Appl. Mech.* 40 (1973) 1107–1109.
23. K. Klotter and G. Kotowski, Über die Stabilität von Lösungen Hillscher Differentialgleichungen mit drei unabhängigen Parametern. *Z. Angew. Math. Mech.* 23 (1943) 149–155.